Development of a cell-free and growth factor-free hydrogel capable of inducing angiogenesis and innervation after subcutaneous implantation

Bruno Paiva dos Santos, Bertrand Garbay, Mathilde Fenelon, Marie Rosselin, Elisabeth Garanger, Sébastien Lecommandoux, Hugo Oliveira, Joëlle Amédée

Author manuscript of article published in Acta Biomaterialia 99, 154-167 (2019) DOI: 10.1016/j.actbio.2019.08.028

Development of a cell-free and growth factor-free hydrogel capable of inducing angiogenesis and innervation after subcutaneous implantation

Bruno Paiva dos Santos[a], Bertrand Garbay[b], Mathilde Fenelon[a,c], Marie Rosselin[b], Elisabeth Garanger[b], Sébastien Lecommandoux[b], Hugo de Oliveira[a], Joëlle Amédée[a]

[a] Tissue Bioengineering Laboratory (BioTis), Inserm U1026, University of Bordeaux, Bordeaux, France

[b] Univ. Bordeaux, CNRS, Bordeaux INP, LCPO, UMR 5629, F-33600 Pessac, France

[c] CHU Bordeaux, Department of Oral Surgery, F-33076 Bordeaux, France

Ph.D. B. Paiva dos Santos[a] bruno.paiva-dos-santos@inserm.fr

Ph.D. H. Oliveira[a] hugo.de-oliveira@inserm.fr

Ph.D. J. Amédée[a] joelle.amedee@inserm.fr

[a] Tissue Bioengineering Laboratory (BioTis), Inserm U1026, University of Bordeaux, 146 rue Léo Saignat, Bordeaux 33076, France.

Prof. B. Garbay[b] bertrand.garbay@bordeaux-inp.fr

Ph.D. M. Rosselin[b] marie.rosselin@enscbp.fr

M.Sc. M. Fenelon[a] mathilde.fenelon@u-bordeaux.fr

Ph.D. E. Garanger[b] elisabeth.garanger@enscbp.fr

Prof. S. Lecommandoux[b] lecommandoux@enscbp.fr

[b] Univ. Bordeaux, CNRS, Bordeaux INP, LCPO, UMR 5629, F-33600, Pessac, France.

Corresponding author:

Ph.D. Bruno Paiva dos Santos

Tissue Bioengineering Laboratory (BioTis), Inserm U1026, University of Bordeaux, 146 rue Léo Saignat, Bordeaux 33076, France

bruno.paiva-dos-santos@inserm.fr

Abstract

Despite significant progress in the field of biomaterials for bone repair, the lack of attention to the vascular and nervous networks within bone implants could be one of the main reasons for the

delayed or impaired recovery of bone defects. The design of innovative biomaterials should improve the host capacity of healing to restore a functional tissue, taking into account that the nerve systems closely interact with blood vessels in the bone tissue. The aim of this work is to develop a cell-free and growth factor-free hydrogel capable to promote angiogenesis and innervation. To this end, we have used elastin-like polypeptides (ELPs), poly(ethylene glycol) (PEG) and increasing concentrations of the adhesion peptide IKVAV (25 % (w/w) representing 1.7 mM and 50 % (w/w) representing 4.1 mM) to formulate and produce hydrogels. When characterized *in vitro*, hydrogels have fine-tunable rheological properties, microporous structure and are biocompatible. At the biological level, 50 % IKVAV composition up-regulated *Runx2*, Osx, *Spp1*, *Vegfa* and *Bmp2* in mesenchymal stromal cells and *Tek* in endothelial cells, and sustained the formation of long neurites in sensory neurons. When implanted subcutaneously in mice, hydrogels induced no signals of major inflammation and the 50 % IKVAV composition induced higher vessel density and formation of nervous terminations in the peripheral tissue. This novel composite has important features for tissue engineering, showing higher osteogenic, angiogenic and innervation potential *in vitro*, being not inflammatory *in vivo*, and inducing angiogenesis and innervation subcutaneously.

Keywords: IKVAV, osteogenesis, neurite outgrowth, sensory neurons, elastin-like polypeptide

1. Introduction

The formation of new blood vasculature from preexisting vessels, a process called angiogenesis, is essential to wound healing. Newly formed blood vessels provide nutrition and oxygen to growing tissues. In addition, inflammatory cells require the interaction with and transmigration through the blood vessel endothelial basement membrane to enter the site of injury. Angiogenesis, in response to tissue injury, is a dynamic process that is highly regulated by signals from both serum and the surrounding specialized extracellular matrix (ECM) environment [1].

Nervous tissue is distributed throughout the organism and is composed of sensory, motor, or mixed neuronal populations. Sensory neurons perceive generally somatic sensations such as pressure, pain, and temperature. These neurons are also involved in smell, vision, taste, and hearing. Motor neurons

ensure the motility of all muscles and glands. Nervous tissue plays an important role in various tissue regeneration and repair contexts although its role is considerably less studied relative to angiogenesis. This can be assessed by surgical denervation or genetic ablation, the effect of these manipulations often resulting in a marked decrease in tissue repair [2, 3].

The development of biomaterials in tissue engineering aims to improve the host healing capacity to restore tissue function. For that, a myriad of strategies of biomaterial design, which includes enriching biomaterials with cells and/or growth factors to improve and stimulate their biological function [4]. Most studies have focused on the formulation of biomaterials that could support just one tissue function, while expecting an entire functional neotissue formation. For example, in bone tissue engineering, the production of biomaterials focuses specially on the osteoblastic function as main actor for bone repair. However, it is well known that it is insufficient to achieve efficient bone repair, and new strategies were developed to bring vascularization function to the biomaterial [5]. However, up to now, the role of nervous system has been largely ignored in the context of bone tissue engineering. Nevertheless, an increasing body of i) physiological, ii) experimental and iii) clinical data supports the role of the nervous system in skeletal development, bone turnover and fracture healing. The peripheral nervous system (PNS) is directly involved in osteogenesis though secretion of neuropeptides, which can stimulate bone cells, modulating their differentiation, function and bone remodeling (formation/resorption) [6-8]. Our previous work using indirect cocultures of rat sensory neurons (SNs) with rat mesenchymal stem cells (MSCs) demonstrates that the SNs modulate osteogenic differentiation of MSCs [9]. It has been also demonstrated that Nerve Growth Factor signaling by sensory nerves coordinates the vascularization and ossification of developing endochondral bone [10]. Finally, several denervation studies have revealed the impact of the PNS on bone development and fracture healing [11, 12]. Taken together, these data should dictate new approaches for developing innovative biomaterials that cannot ignore the function of vascular and nervous tissues in the skeletal system. The polymer chemistry should be one relevant issue to design such biomaterials and to functionalize them to render them permissive to different cell types.

Hydrogels exhibit great resemblance to the extracellular matrix, which makes them essential candidates for tissue engineering applications. In addition, they can be easily functionalized with bioactive molecules to confer specific properties to the scaffold, such as attraction of specific cell types to improve tissue repair (vascularization, innervation…). Hydrogels can be formed by either covalent or physical bonding. Both approaches raise several issues concerning the material processing or its mechanical properties. As a matter of fact, hydrogels should meet several criteria: (i) they should be biocompatible, and should not induce adverse inflammatory or allergic responses; (ii) their polymerization should be achieved by simple technologies, avoiding the use of toxic chemical cross-linkers; (iii) the grafting of different signaling molecules for angiogenesis and innervation purposes should be attainable using simple procedures, and the concentration of each signaling molecule should be finally tuned; (iv) production and purification of the polymer that will form the hydrogel should be at reasonable costs, performed by robust technologies that are already used by the pharmaceutical industry, scalable, and compatible with GMP production for future pharmaceutical production.

According to these requirements, elastin-like polypeptides (ELPs) meet these criteria [13, 14]. ELPs are recombinant peptide polymers, derived from (tropo)elastin, that consist of multiple repeats of Val-Pro-Gly-Xaa-Gly pentapeptides (VPGXG), where Xaa (X) represents a guest amino acid residue [15]. The nature of the Xaa residue strongly affects ELPs' physico-chemical properties, in particular hydrophilicity, charge, and lower critical solution temperature (*LCST*) [16, 17]. ELPs are especially attractive polymer scaffolds for tissue engineering as they can be engineered to approach the viscoelastic properties of native elastin and can be produced with excellent reproducibility in large scale [18, 19]. In addition, they are biocompatible, biodegradable, and can be purified without the need for complex and expensive chromatographic steps [16]. To increase the versatility of recombinant ELP-containing scaffolds, our group recently developed dual biotechnological and synthetic approaches. Post-modifications using chemoselective bioconjugation reactions at methionine at the guest residue position are in particular used to tune the properties of recombinant

ELPs and/or to introduce specific reactive groups [20-22]. The latter can be subsequently reacted to introduce specific bioactive motifs (e.g., cell-specific peptide sequences) or to control cross-linking density. Altogether, the remarkable properties of ELPs make them very attractive as biomaterials for tissue engineering applications.

In the present work, conscious of the complexity and heterogeneity of the innervated and vascularized tissue, we have formulated hydrogels from cross-linked ELP scaffolds, branched poly(ethylene glycol) (PEG) and IKVAV, a laminin-derived adhesion peptide capable to sustain neurite outgrowth and angiogenesis. Hydrogels with different compositions (*i.e.*, PEG to IKVAV ratio) were first characterized in terms of rheological properties and porosity. The cellular responses (metabolic activities, phenotypes) of mesenchymal stromal cells (MSCs), endothelial cells (ECs) and sensory neurons (SNs) were then evaluated in vitro. The best performance composition was finally implanted subcutaneously in mice to assess the induction of angiogenesis and innervation in peripheral tissue.

2. Material and Methods

2.1. Hydrogel production

The ELP used for the formulation of hydrogels was prepared by a dual biosynthetic and chemical strategy. The recombinant ELP with the sequence MW[VPGVG-VPGMG-$(VPGVG)_2]_{10}$ was produced in *Escherichia coli* bacteria and purified by inverse transition cycling as described previously [20]. Methionine residues (11 total) were subsequently thioalkylated chemoselectively and quantitatively with 1-allyloxy-2,3-epoxypropane providing 11 alkene groups for subsequent thiol-ene photo-cross-linking reactions [22] (Figure 1A). Four-arm thiol-ended PEG (20 kDa) was purshased from JenKem, USA. The laminin-derived adhesion peptide sequence Cys-βAla-Ile-Lys-Val-Ala-Val-βAla-Cys (CβA-IKVAV-βAC, thereafter noted IKVAV) and the control scrambled sequence Cys-βAla-Val-Lys-Ala-Ile-Val-βAla-Cys (CβA-VKAIV-βAC, thereafter noted VKAIV) were purchased from Biomatik Corporation, Canada.

Hydrogels were formulated with ELP and variable amounts 4-arm SH-PEG and IKVAV (or VKAIV) at equimolar ratios of thiol to alkene. Photo-cross-linking was achieved using the photoinitiator Irgacure® 2959 (ref 410896, CAS Number: 106797-53-9, Sigma-Aldrich) (0.05 % w/v) exposure to UV light (λ=305 nm) (Figure 1B). Three hydrogel compositions were evaluated: (*i*) ELP + PEG, (*ii*) ELP + 25 mol % IKVAV or VKAIV (corresponding to a final concentration of 1.7 mM) + 75 mol % PEG, and (*iii*) ELP + 50 mol % IKVAV or VKAIV (corresponding to a final concentration of 4.1 mM) + 50 mol % PEG. (Figure 1C) A schematic representation of hydrogels' composition is shown in Figure 1A-C. For both *in vitro* and *in vivo* biological evaluations, hydrogels were produced, incubated overnight in PBS 0.01 M and then used in the experiments. All experiments were performed with hydrogels hydrated and previously crosslinked.

2.2. Rheological properties

Hydrogels were soaked for 24 h in phosphate buffer saline (PBS) 0.01 M pH 7.4 prior to the determination of the storage (G') and loss moduli (G"). Frequency sweeps were performed at a constant strain (0.1 %) in the angular frequency range 0.1–100 rad/s in a Kinexus pro$^+$ rheometer (Malvern Instruments, UK). The mechanical characterization was performed on ELP + PEG composition at different hydrogel concentrations (*i.e.* 5 %, 7.5 %, and 10 % (w/w)) and ELP + 50 % IKVAV at 7.5 % (w/v). Measurements were performed at 37 °C.

2.3. Scanning Electronic Microscopy

To visualize the hydrogel microstructure and determine the pore size, cryo-scanning electron microscopy (cryo-SEM) analysis was performed. The hydrogel preparations were mounted on a slit holder, plunged into liquid nitrogen slush and then transferred into the Gatan Alto 2500 (Pleasanton, CA, USA) pre-chamber cooled to -100 °C where vacuum was created. After cutting samples with a cold blade, the water content was sublimated until – 40 °C for up to 5 min, and then sputter coated for 120 s with gold-palladium. The samples were then transferred to the microscope cryo-stage (approximate temperature: -150 °C) for imaging. The morphology was characterized by SEM (JEOL

JSM- 6700F) using SEI and LEI detectors operating at 10 kV accelerating voltage, with approximately 15 mm working distance and the magnifications varied between 250 x and 5,000 x. Images of at least four different regions from one hydrogel of each composition were taken. ImageJ software was used to calculate the apparent pore size of all hydrogel compositions. The average of two perpendicular measures for each pore was used ($63 < n < 85$).

2.4. *In vitro* degradation

15 µL of each hydrogel formulation (n=6) were incubated in 150 µL solution of proteinase K (0.5 U/mL) (Amresco, #0706) in 50 mM Tris Base, 1 mM EDTA, 5 mM $CaCl_2$ and 0.5 % (v/v) Triton X-100 (pH 8.0) for 7 h at 37 °C. The free primary amine group content, expressed as the number of free amine groups presents per 1000 amino acids (n/1000), was determined using 2,4,6-trinitrobenzenesulfonic acid (TNBS) [23]. Briefly, 200 µL of a freshly prepared 0.5 % (w/v) TNBS (Sigma-Aldrich®) solution in distilled water were added to the samples. After an incubation of 2 h at 40 °C, 600 µL of 6 M HCl was added, and the temperature was raised to 60 °C for 30 min. A control was prepared applying the same procedure except that HCl was added before the addition of TNBS. The free amine group content was calculated using a molar absorption coefficient of 14,600 l/mol/cm for trinitrophenyl lysine [24].

2.5. Cell isolation and cultures

Primary sensory neurons were obtained from dorsal root ganglion (DRG) from healthy 5-9 weeks old Wistar rats as described elsewhere [25]. Briefly, spinal columns were removed and opened from the caudal to the rostral in order to expose the DRGs. They were individually harvested and digested with 1 mg/mL Collagenase Type IV (Gibco®) for 2 h at 37 °C. Subsequently, digestion product was washed twice with culture medium supplemented with 2 % (v/v) B-27 Serum-Free Supplement® (B-27, Gibco®), 1 µM cytarabine and 1 % (v/v) Penicilin Streptomycin and mechanically dissociated using fire-polished glass Pasteur pipettes (full diameter and ½ diameter). The cell suspension was finally

washed three times with medium, and resuspended in culture medium. Neurons were seeded immediately after isolation at a density of 50,000 cells/cm^2.

Bone marrow MSCs were isolated from healthy 6-10 week-old Wistar rats. Briefly, femur and tibia were removed and cut on the extremities to expose the bone marrow. Bones were transferred to 1.5 mL tubes and centrifuged at 1500 x g for 30 s, to flush the bone marrow. The obtained pellet was resuspended in Dulbecco's Modified Eagle's Medium low glucose (DMEM, Gibco®) supplemented with 10 % (v/v) fetal bovine serum (FBS, PANTM-Biotech, Aidenbach, Germany) and 1 % (v/v) Pen/Strep and carefully passed through 16 G and 21 G needles for 4-6 times. The content from a femur and a tibia was seeded in a 75 cm^2 flask and incubated in humidified incubator (37 °C and 5 % CO2). Culture medium was changed twice a week to remove non-adherent cells. Adherent cells were cultured until reaching 90 % of confluence, and then transferred to a larger surface. Cells were used until passage 3 and seeded on the hydrogels at 20,000 cells/cm^2. MSCs were cultured in osteogenic media, which is the before mentioned culture medium (DMEM, Gibco®) supplemented with 10^{-9} M dexamethasone (Sigma-Aldrich®), 10 mM β-glycerophosphate (Sigma-Aldrich®) and 50 µg/mL ascorbic acid (Sigma-Aldrich®).

Bone marrow-derived endothelial cells (ECs) were purchased from Cell Biologics ® (catalog number RA-6221). Cells were cultured with endothelial cell growth medium-2 (EGM-2; Lonza-Verviers, France) in gelatin-coated (2 % (w/v)) plates containing all bullet kit supplements and 5 % (v/v) FCS (GIBCO Life Technologies, Karlsruhe, Germany) and incubated at 37 °C in humidified atmosphere with 5 % CO_2. Cells were used until passage 7 and seeded on the hydrogels at 20,000 cells/cm^2. For both sensory neurons and MSCs isolation, the use of rats as experimental models was approved by the Bordeaux University Animal Ethics Committee (APAFIS#4375-2016030408537165 v4).

2.6. Metabolic activity

Metabolic activity of SNs, MSCs and ECs cultured in hydrogels (n=5) was measured using a resazurin-based assay [26]. Briefly, cells were seeded onto 7.5 % (w/v) hydrogels at a density of 50,000 cells/cm² for SNs or 20,000 cells/cm^2 for ECs and MSCs in a 96 well plate. 150 µL of culture medium containing resazurin (0.01 mg/mL) was added to each well and the microplate was incubated at 37 °C for 3 h. Subsequently, 100 µL of supernatant was transferred to another 96 wells microplate and fluorescence was measured (exc = 530 nm, em = 590 nm, Victor X3, Perkin Elmer). Metabolic activity was measured at days 4 and 7.

2.7. Confocal Microscopy

Cells were fixed with 4 % (w/v) paraformaldehyde at 4 °C for 30 min, permeabilized with Triton X-100 at 0.1 % (v/v) for 30 min at 4 °C, blocked with BSA 1 % (w/v) for 1 h. For SNs, rabbit anti-rat beta III Tubulin antibody (Abcam) was used at a dilution 1:500 and second antibody goat anti-rabbit IgG conjugated with Alexa Fluor 488 (Molecular probes) at 1:400 dilution for 2 h at room temperature. For MSCs and ECs, filamentous actin was labeled with phalloidin conjugated with Alexa Fluor 568 (Molecular probes). Nuclei were labeled with DAPI (4', 6'-diamidino-2-phenylindole, Fluo Probes) at 1 µg/mL for 10 min at room temperature. Samples were visualized using a confocal laser-scanning microscope (SPE, Leica Microsystems). Neurite length was measured using Image J, using "Simple Neurite Tracer" tool. Neurite length was measured using Image J, using "Simple Neurite Tracer" tool. Neurites (n=5 samples for ELP + PEG composition and 12<n<30 for all other compositions) were measured tracing a path from the soma to the visible end and the length was converted in µm.

2.8. RNA extraction, cDNA synthesis and gene expression analysis

Total RNA was extracted from cells after 7 days of culture in the 7.5 % (w/v) hydrogels by using the RNeasy® Plus Micro Kit (Qiagen, Hilden, Germany) according to the manufacturer's protocol. RNA final concentration and purity (OD 260/280) was determined using a Nano Photometer® P 330 (Implen GmbH, Munich, Germany). 100 ng of total RNA from the pool of 5 wells were reverse transcribed into cDNA using the Maxima Reverse Transcriptase kit (Thermo Scientific™, Thermo

Fisher Scientific, Waltham, MA, USA), according to the manufacturer's protocol. RT-qPCR experiments were performed using a Takyon ROX SYBR 2X MasterMix dTTP blue (Kaneka Eurogentec S.A., Belgium) using standard PCR conditions for Sybr Green ® detection in a CFX Connect™ Real-Time PCR Detection System (Bio-Rad Laboratories, Hercules, CA, USA) and analyzed with the CFX Manager™ software, version 3.0 (Bio-Rad Laboratories). Primer sequences are presented in Table 1. Target gene expression was quantified using the cycle threshold (Ct) values and relative mRNA expression levels were calculated according to 2^{-DDCt} method using the ELP + PEG composition as reference (n>4).

2.9. Subcutaneous implantation in mice

50 % IKVAV and the scrambled composition cell-free hydrogels were produced in a volume of 50 µL and thereafter implanted into both dorsal subcutaneous sites of 9 weeks old female Balb/c mice (central animal facility of the University of Bordeaux, Bordeaux, France) under gas anesthesia (isoflurane). Six independent materials were implanted per hydrogel composition and per time point. Animals were sacrificed at 2 and 4 weeks. All the procedures for mice handling were based on the principles of Laboratory Animal Care formulated by the National Society for Medical Research and approved (ref A33063917) by the Animal Care and Experiment Committee of University of Bordeaux, Bordeaux, France. Experiments were carried out in accredited animal facilities following European recommendations for laboratory animal care (directive 2010/63/EU and decree #2013-118 of 1st February 2013 from the French Government).

2.10. Histology and Immunohistochemistry

Samples were harvest with the surrounding tissue, fixed with 4 % (w/v) paraformaldehyde for 48 h at 4 °C and embedded in paraffin. Eight microns sections were cut and stained with Hematoxylin and Eosin using standard protocols and observed under a photomicroscope (Nikon eclipse 80i, The Netherlands). Immunohistochemistry for vessel structures were performed using CD31 and for nervous structures using β III tubulin. Antigen recovery was performed using a citrate buffer and

primary antibodies were against CD31 (Abcam, ab28364) (1:100), β III tubulin (Abcam, ab41489) (1:1000). For CD31, the secondary antibody used was from Impress kit (VectorLabs, USA, MP-7401), used according to the manufacturer's instructions. Specific staining was revealed using the 3,3'-diaminobenzidine staining solution (VectorLabs, USA). Counterstaining was performed using Mayer's haematoxylin. Samples were then mounted using Pertex medium (Sigma). For β III tubulin, goat anti-chicken Alexa Fluor® 488 (1:200) were used. Counterstaining was performed using DAPI (Thermo Scientific™, Germany) (1:1000) and samples were mounted using Fluoromount Gold G (Thermo Scientific™, USA). Sample imaging was performed using a microscope (Nikon Eclipse 80i) equipped with a digital camera (Nikon Dxm 1200C) or a confocal laser-scanning microscope (SPE, Leica Microsystems). For vessel and nervous structures evaluation, histological slides were scanned in a Nanozoomer 2.0 HT with fluorescence imaging module (Hamamatsu Photonics France) using objective UPS APO 20X NA 0.75 combined to an additional lens 1.75X, leading to a final magnification of 35X. Virtual slides were acquired with a TDI-3CCD camera and analysed on NDPView® software. Fluorescent acquisitions are done with a mercury lamp (LX2000 200W - Hamamatsu Photonics, Massy, France) and the set of filters adapted for DAPI and Alexa 488 fluorescence. Structures positive-stained for CD31 and β III tubulin were manually counted inside the surface between the hydrogel structure and the most external flat nuclei identified surrounding the hydrogel.

2.11. Statistical analysis

Using the Graphpad Prism 5.0 software, statistically significant differences between several groups were analyzed by Kruskal-Wallis or ANOVA tests, followed by a Dunett or Bonferroni post-test, respectively. The non-parametric Mann-Whitney test was used to compare two groups. A *p* value lower than 0.05 was considered statistically significant.

3. Results

3.1. Hydrogel characterization

As expected, after crosslinking, ELP + PEG hydrogels were transparent [20] (Figure 1B) allowing microscopic analysis after cell seeding. The other formulations regardless of adhesion peptide sequences with the respective concentrations (Figure 1C) were transparent too (Supplementary Figure 1), demonstrating the good homogeneity of the biomaterials. Since we aimed to produce hydrogels to induce innervation, the substrate stiffness should have storage modulus 1 kPa < G' < 1.5 kPa. Indeed, this range has been shown to be optimal for DRG SNs outgrowth [27]. Here, we observed that storage modulus increased proportionally to the final hydrogel concentration (sum of all hydrogel solid components represented in % w/w) (Figure 1D), and the 7.5 % (w/v) final mass concentration presented a storage modulus in this range. We used this final concentration for the rest of our study.

To assess hydrogels structure, hydrogels were observed by SEM. All compositions exhibit microporous structure (Figure 2A), with pore sizes varying from 11 ± 2 µm (25 % IKVAV) to 16 ± 3 µm (50 % IKVAV). Hydrogels functionalized with the same concentration of adhesion peptide had similar pore sizes. Moreover, the hydrogel containing 25 % of adhesion peptides had smaller pore sizes than those containing ELP + PEG or 50 % of adhesion peptides ($p<0.001$) (Figure 2B).

To evaluate if reticulation lowers the material biodegradability, we incubate all compositions with proteinase K. Free primary amines in solution were detected in all samples studied, indicating that the reticulation process did not interfere with the *in vitro* degradation property. Formulations with the same concentration of adhesion peptide did not differ between themselves. Hydrogel formulations containing 50 % adhesion peptides had higher values of free primary amines in solution relative to those containing 25 % adhesion peptides ($p<0.05$) and ELP + PEG composition ($p<0.001$). Enzymatic degradation seems to increase proportionally to the protein content (Figure 2C).

3.2. *In vitro* evaluation

To analyze the hydrogel cytocompatibility, rat primary MSCs, ECs and SNs were cultured for 7 days, and we measured their metabolic activity. All hydrogels tested enabled attachment and culture of

the different primary cells tested (Figure 3). There is no difference in MSCs metabolic activity between the hydrogel compositions. For ECs, metabolic activity was higher in 25 % IKVAV compared to the respective scrambled control ($p<0.05$). For SNs, ELP + PEG composition resulted in lower cell metabolic activity relative to all other compositions ($p<0.001$). Moreover, the 50 % IKVAV induced higher metabolic activity relative to 25 % IKVAV ($p<0.05$) and 50 % VKAIV ($p<0.01$). Interestingly, we observed that SNs metabolic activity increases proportionally to the IKVAV concentration.

To assess if hydrogel compositions could support MSCs differentiation, they were cultured in osteogenic medium for 7 days. We observed that cells formed spheroid aggregates for all compositions (Figure 4A). We also analyzed gene expression of a panel of osteogenic markers: *Runx2* and *Sp7* as early-stage differentiation markers, and *Spp1* (Opn) as a late-stage marker. In addition, we analyzed key factors for the bone repair process, which induce vascularization and osteoblast differentiation: *Vegfa* and *Bmp2*, respectively (Figure 4B). For the osteogenic markers, *Runx2* was upregulated in 50 % IKVAV composition relative to ELP + PEG ($p<0.01$). For Osx, there was an upregulation of 50 % for both IKVAV ($p<0.001$) and VKAIV-containing gels ($p<0.01$) compare to ELP + PEG. In addition, Osx was upregulated in 50 % IKVAV relative to 25 % IKVAV ($p<0.05$). For Opn, there was an upregulation in 50 % IKVAV relative to ELP + PEG ($p<0.001$), 25 % IKVAV ($p<0.01$) and 50 % VKAIV ($p<0.001$). Opn was also upregulated in 25 % IKVAV relative to ELP + PEG ($p<0.05$). For the angiogenic factor *Vegfa*, it was upregulated in 50 % IKVAV relative to ELP + PEG and 50 % VKAIV (both $p<0.05$). For *Bmp2*, both 50 % IKVAV and 25 % VKAIV were upregulated relative to ELP + PEG ($p<0.001$ and 0.05, respectively). Interestingly, all genes were upregulated in 50 % IKVAV relative to ELP + PEG and the upregulation of all genes was proportional to the IKVAV concentration.

As means to evaluate the proangiogenic potential of these hydrogels, we cultured primary rat bone marrow ECs within the different hydrogel compositions. After 7 days, ECs behaved distinctly according to concentration of adhesion peptides. In ELP + PEG composition, ECs formed isolated cellular aggregates and planar structures. In 25 % IKVAV or VKAIV-containing hydrogel compositions, ECs behaved similarly organizing themselves in monolayers. For the 50 % IKVAV-containing

compositions, ECs are organized in a branched-like structure, with the presence of some segments and branched points. In the case of the control peptide (50 % VKAIV) representative images revealed that the cells formed also some segments and branched points, but that other cells seemed to maintain a cobblestone organization (Figure 5A).

We also assessed the ECs gene expression of important genes, which play a role during vessel formation (*Angpt1* and *Tek*) and extracellular matrix remodeling (*Mmp2*) (Figure 5B). We observed an upregulation in *Tek* in 50 % IKVAV composition relative to ELP + PEG and to the scrambled VKAIV composition (both $p<0.05$). For *Angpt1* and *Mmp2*, no significant difference in gene expression was observed.

For SNs, cells exhibited very distinct behavior according to hydrogel compositions (Figure 6). In ELP + PEG composition, cells formed larger cellular aggregates and neurites were not spread, but were wrapped around the cell bodies. When the IKVAV sequence was added to the hydrogel composition, neurites could outgrow. ELP + PEG composition induce the formation of shorter neurites relative to 25 % IKVAV ($p<0.01$), 50 % IKVAV ($p<0.001$) and 50 % VKAIV ($p<0.001$). In addition, 50 % IKVAV formed the more complex neurite network with longer neurites relative to all other compositions ($p<0.001$). Interestingly, the average neurite length increased proportionally according to IKVAV concentration.

3.3. *In vivo* evaluation

Based on the performance of the 50 % IKVAV composition analyzed *in vitro* with ECs and SNs, we evaluated the inflammatory response of this hydrogel composition, its ability to induce angiogenesis and innervation *in vivo* upon subcutaneous implantation in mice, and compared it with the scrambled peptide formulation (50 % VKAIV). As observed in Figure 7, no signal characteristic for major inflammation could be observed. The hydrogel was still detectable (asterisks), surrounded by an unstructured tissue, and limited by a thin layer of flat nucleated cells (dashed line). Quantification of vessels and nervous structures were made inside this area, because it surrounds the hydrogel and

therefore represents the direct host tissue reaction. When we quantified the angiogenesis (by immunohistochemistry of CD31), there was no difference in vessel density between IKVAV and the scrambled peptide after 11 days of implantation (vessels indicated by white arrowheads). However, after 26 days of implantation, the density of vessels was higher in IKVAV composition relative to the scrambled ($p<0.05$) (Figure 8). In addition, there is an increase in vessel density over time in IKVAV ($p<0.05$), while there is no difference in vessel density over time with the scrambled composition. For the innervation potential, nervous structures were assessed by immunohistochemistry of βIII tubulin. No nervous structures were found surrounding the VKAIV-containing hydrogel. We detected only nervous structures surrounding the IKVAV-containing hydrogel, reinforcing the role of IKVAV on neurons recruitment and neurites outgrowth. When we quantified the density of nerves structures (the number of nervous structures per area surrounding the implant), it seemed to increase over time, similarly to what was observed for angiogenesis. We observed 1.3 ± 0.9 nervous structures/mm² after 11 days of implantation and 8 ± 4 nervous structures/mm² after 26 days, considering only the region surrounding the implant. The same tendency occurred for the surface of these nervous structures, being 136 ± 111 µm² after 11 days of implantation and 1191 ± 916 µm² after 26 days.

4. Discussion

Despite the development of new scaffolds and the progress of technologies for their biofabrication, only a few of them are designed to integrate the complexity and the heterogeneity of a tissue composed of multiples cell types and functions. This is particularly needed for engineering vascularized and innervated biomaterials that will be used to replace connective tissues such as skeletal tissues. In order to generate neurovascular networks within an implant, specific functions are required for facilitating the formation of vascular structures as well as the axonal growth of neuronal cells. In such context, biomaterial properties should be carefully selected according to these functions.

Here, we have developed an ELP-containing hydrogel that fulfills the requirements. The versatility of ELP-containing biomaterials and their use as scaffolds for tissue regeneration have been already demonstrated. They have aroused great interest as a biomaterial for tissue engineering on account of their biocompatibility, biodegradation and their multiple chemical modifications that can provide diverse features.

A common strategy to add a biological and specific function to biomaterials is to use adhesion motifs of proteins from the extracellular matrix in order to attract specific cell types. Several motifs are used in tissue engineering to promote ECs adhesion and proliferation, such as REDV, RGD and GRGDSP which are derived from fibronectin, IKLLI, IKVAV, PDSGR and YIGSR, derived from laminin, and also DGEA from collagen type I [28]. Concerning neurons attachment and neurite outgrowth, laminin has received particular attention. Several bioactive epitopes have been identified in laminin sequence, including YIGSR, RNIAEIIKDI and especially IKVAV, which were described to promote cell attachment and/or neurite outgrowth and axon guidance [29, 30]. It was recently demonstrated that inclusion of IKVAV within a scaffold is known to enhance cell adhesion of neurons, as well as neuronal differentiation in both 2-dimensional and 3-dimensional environments [reviewed in [31]] .

Moreover, it has been also admitted that the same sequence also support blood vessel formation, activate endothelial cell adhesion and function [32] and induce vessel formation [30, 33, 34]. Aiming the development of a neurovascular implant, this peptide was then selected as support for the two corresponding cell types.

Interestingly, MSCs responses to the IKVAV-containing hydrogels evidenced that this hydrogel is also permissive to osteogenic differentiation of MSCs, which constitute an additional value with the perspective for engineering an innervated vascularized bone material. This osteoconduction property of IKVAV peptide was already reported by Frith et al. (2012) [35]. The combination of properties encompassing different tissues makes IKVAV an interesting candidate to increase biological function to biomaterials [recently reviewed in [36]].

The versatility of ELPs is closely related to their unique ability for controlled chemical modifications. When associated to different peptide sequences and in different concentrations, ELPs can exhibit diverse properties. Here, we produced ELPM40 combined with PEG, and grafted adhesion peptides (IKVAV and the scramble sequence VKAIV) in different concentrations, ranging from 0 (PEG), 1.7 mM (25 % peptide) and 4.1 mM (50 % peptide). The grafting of peptides in the ELP backbone represents a versatile strategy to change the biological signal as well as its concentration without the need to modify the ELP backbone sequence by tedious molecular cloning techniques.

We first characterized the physicochemical properties of the hydrogels. They were microporous and enzymatically degradable (Figure 2), indicating that the crosslinking process did not prevent the *in vitro* degradation property. Expectedly, the hydrogel degradation was proportional to the protein content. Enzymatic degradation is an important property for materials with biomedical application. *In vivo*, different cell types must be able to enter into the hydrogel structure to colonize it. The common mechanism for cell migration is the secretion of proteases that digest the hydrogel structure at a low rate, and therefore allows cellular colonization and function [37]. Regarding the porosity, the average pore size of the hydrogels greatly affects the growth and invasion of cells within its 3D structure. Indeed, several reports have shown that different regeneration processes rely on different pore sizes, with an optimum pore size of 5 µm for neovascularization, 5–15 µm for fibroblast ingrowth, 100–350 µm for the regeneration of bone and 40–100 µm for osteoid ingrowth [38]. Thus, the control of scaffold porosity and microarchitecture is a key factor for the regulation of the engineered tissue properties.

Regarding cellular behavior, three different cell types were studied due to their interest in tissue engineering: (i) MSCs due to their differentiation potential, (ii) ECs because of their pivotal role in angiogenesis, and (iii) SNs to demonstrate the capacity of the nervous tissue to adhere and to outgrow neurites. For all of these cell types, the different hydrogel formulations permit adhesion and culture. The photoreticulation agent, Irgacure® 2959 (ref 410896, CAS Number: 106797-53-9, Sigma-Aldrich), used in our study at 0.05 % (w/v) has already been shown to be cytocompatible [39].

When MSCs were associated with hydrogels, cells formed cellular aggregates for all compositions (Figure 4A). This cellular organization has already been related to an increased osteogenic potential in MSCs [40]. In addition, MSCs also formed spheroids when cultured on ELP-based coating plates, presenting an increase of classic early and late osteogenic markers as well as mineralization process [41]. Another study evaluated the coating of titanium alloys with ELP-containing RGD adhesion sequence, and the authors observed that MSCs had an earlier upregulation of osteogenic markers, indicating faster osteogenic differentiation and mineral deposition on adhesive ELP coatings [42]. Taken together, these results suggest that ELP is an osteoconductive substrate for MSCs.

When we assess MSCs gene expression, a panel of genes that play a role during different stages of osteogenic differentiation [43, 44] were upregulated in 50 % IKVAV, revealing more intense cell commitment in this composition. Interestingly, the expression of *Bmp2* and *Vegfa* were also upregulated in these MSCs cultured within the 50 % IKVAV. Both genes orchestrate bone repair, triggering osteogenic differentiation, inducing angiogenesis, promoting neuronal migration, neuronal survival and axon guidance [45-50]. All genes analyzed were upregulated in a dose-dependent manner relative to the IKVAV concentration. In the literature, the IKVAV sequence has already been shown to have important effects in MSCs: supporting the osteogenic differentiation [35, 51], increasing cell proliferation in a dose-dependent manner, with this effect being regulated by ERK1/2 and Akt signaling pathways [52]. Indeed, these signaling pathways are strongly related to the osteogenesis process, activating the transcriptional factors Runx2 and Osx [53-56] that were upregulated in our 50 % IKVAV composition. Taken together, these data suggest that the 50 % IKVAV can directly support osteogenesis, in a coupled manner with angiogenesis and innervation.

Interestingly, we observe an upregulation of *Sp7* and *Bmp2* when MSCs were cultured, respectively, in both VKAIV compositions and 25 % VKAIV relative to ELP + PEG. To our knowledge, there are no study evaluating the effect of the VKAIV sequence on the osteoblastic differentiation of MSCs. In our study, VKAIV-containing compositions, used as a negative control formulation, cannot induce the upregulation of all the osteogenic markers involved in the different stages of osteogenesis process

(upregulation of *Sp7* and *Bmp2* but not *Runx2* and *Spp1*, Figure 4B), suggesting not to have a well-defined role in this process. The upregulation of some osteoblastic genes in VKAIV-containing hydrogels can be explained by the cellular organization as spheroids. Our group has already shown that spheroid organization can provide numerous cellular contacts, stimulating junctional proteins such as connexin 43 or pannexins that could drive the osteogenic differentiation of MSCs [57, 58]. Further studies are needed to clarify if MSCs are sensitive to VKAIV sequence and if it has an effect on MSCs differentiation.

When ECs were cultured in hydrogels, we observed distinct behavior according to formulations. These differences could be explained by (i) sequence of the adhesion motif, using the biologically functional IKVAV or the scrambled sequence VKAIV, which is supposed to have no biological activity [59]; and (ii) the charge of the hydrogel surface, being a consequence of the increase of the adhesion peptide concentration. The substrate charge is known to change adsorption of molecules to the hydrogel surface. In addition, it has already been reported that ECs respond differently according to substrate charge [60]. In 50 % IKVAV composition, cells were distributed in aggregates that fused forming long and branched structures. This can represent an increased potential of this hydrogel to induce angiogenesis. In fact, since 90's Kleinman's group reported the angiogenic potential of IKVAV *in vivo* [33, 34, 61]. Grant and colleagues demonstrated increased ECs mobilization, capillary branching, and vessel formation in a murine and chick yolk sac/chorioallantoic membrane *in vivo* assays [61]. Kibbey and colleagues observed an angiogenic effect in a dose-dependent manner and, when the SIKVAV-containing peptide was injected with melanoma cells, the peptide induced vascularization and tumor growth [33, 34]. Concerning ECs gene expression, we observed a significant upregulation of *Tek* in the 50 % IKVAV composition. We also analyzed the expression of *Angpt1*, a ligand of Tek, which was not significantly upregulated in the 50 % IKVAV. Angpt1 acts as an agonist, causing rapid receptor transphosphorylation, leading to subsequent downstream activation of the protein kinase B/Akt/FKHR (FOX01) pathway to promote ECs survival. These molecules are

closely related in the control of angiogenesis, playing a role in the enlargement of existing vessels, and are essential for vascular maturation and stability.

For SNs, the 50 % IKVAV composition induced a wider neurite network, and the longest average neurite length. This effect was specific to the peptides IKVAV, and was dose-dependent. Some other studies have evaluated rat primary SNs neurite length, mostly in 2D. Liu and colleagues (2013) compared two isolation methods for embryonic rat SNs from DRGs and they observed neurite length between 200 - 250 μm at day 7 when the culture medium was supplemented with 50 ng/mL of NGF [62]. Sepehr and colleagues (2009) assessed the sensitivity of SNs from DRGs in different glucose concentration media after 24 h of culture with 50 ng/mL of NGF. They found neurite length ranging from 229 ± 20 μm (for SNs isolated from 6 days old rats cultured in 6 mM glucose medium) to 301 ± 31 μm (for SNs isolated from 4 days old rats cultured in 15 mM glucose medium) [63]. Repic and colleagues (2016) observed that SNs from adult rats on glass had 200 - 300 μm length on day 3 in a culture with 100 ng/mL of NGF [64]. Ladak and colleagues (2011) studied the impact of MSC-derived Schawnn cells and undifferentiated MSCs on embryonic rat DRGs in indirect co-culture system without growth factors supplementation. In the case of SNs without any co-culture conditioning, they observed that neurite length reached 130 ± 22 μm after 48 h of culture [65]. In a 3D environment, Kim and colleagues (2015) measured the SN neurite length of 6-9 months rats in collagen hydrogel. Neurites reached a length of 229 ± 103 μm when SNs were cultured in the absence of any growth factor [66].

In opposite to these publications, it is important to emphasize that in our study we did not supplement the culture medium with any growth factors such as nerve growth factor (NGF). It is already known that NGF is an important neurotrophins for the development of the peripheral nervous system, which stimulates neurite outgrowth and neurons survival [67]. We did not use NGF nor other neurotrophin because we wanted to investigate the particular impact of the hydrogel structure and composition on neurite outgrowth. According to our results, the average neurite length

in 50 % IKVAV composition was 266 ± 64 µm, which is similar to the length measured in the aforementioned studies that used NGF supplementation.

After subcutaneous implantation, both 50 % IKVAV and 50 % VKAIV compositions did not trigger major signals of inflammation. Moreover, we did not detect the presence of multinucleated giant cells. *In vivo* biocompatibility of ELP hydrogels has already been shown by others [68]. The hydrogel structure was still detectable (indicated by asterisks, Figure 7), with minimal cellular invasion probably due to small pore sizes of our gels (around 15 µm). When we quantified the blood vessels within the surrounding region of implantation, we observed a higher density of vessels in IKVAV composition relative to the scrambled VKAIV composition after 26 days of implantation, and the density of vessels increased over time (Figure 8). These results are supported by the *in vitro data* and ECs gene expression, which showed *Tek* upregulation in 50 % IKVAV composition. Considering the absence of multinucleated giant cells, which are often associated with increased angiogenesis mainly due to Vegf secretion, and the previous reports on the role of IKVAV in angiogenesis, we conclude that the increase in vessel density is due to the hydrogel composition and not to a secondary process. For the innervation potential, nervous structures were only observed in the IKVAV composition for both time points, supporting our *in vitro* results with SNs and reinforcing the role of IKVAV on neurons recruitment and neurites outgrowth. The density of nervous structures and their surface also seemed to increase over time. Considering the minimal cellular invasion in the hydrogels and the high vessel and nervous structures density surrounding the implantation, we can hypothesize that both processes are induced during the development of the unstructured tissue, probably due to the degradation of the hydrogel structure, which would make the IKVAV epitope available to the surrounding cells. In addition, we performed rheological analyses of 50 % IKVAV and VKAIV at different time points in order to check if hydrogels have distinct behavior over time. We analyzed the rheological properties i) in vitro after 1, 11 and 26 days in a physiological solution (PBS 0.01 M), and in vivo after 26 days of implantation in subcutaneous implantation. There is a slight decrease in storage modulus for both compositions (see Supplementary Figure 2), suggesting that they the same

in vitro and in vivo degradation behavior. Nevertheless, 50 % IKVAV implant presented a superior vessel formation and innervation potential in vivo after 26 days, reinforcing this effect to its biological function.

However, we can identify some important points and limitations for this hydrogel production strategy. For hydrogel formulations, the concentration of ELPM40 changes between ELP + PEG, ELP + 25 % adhesion peptide and ELP + 50 % adhesion peptide compositions. The changes in ELPM40 concentration happen due to stoichiometric reasons, keeping the equimolarity of alkene and thiol groups in ELPM40 and adhesion peptides + SH-PEG, respectively. Conscious of ELPM40 and SH-PEG concentration variation dependent of IKVAV concentration, we decided to use as an appropriate control the scrambled peptide (VKAIV) grafted within the hydrogels. For biological response, an effective cellular organization in 3D as well as pores interconnectivity were not proved *in vitro*. We observe that cells do not directly colonize hydrogels *in vivo*. A faster and more effective induction of angiogenesis and innervation could be enhanced by increasing the pore sizes and pore interconnectivity of our hydrogels. In addition, in a further perspective, the biological functionality of hydrogels can be increased by adding other components. For example, in order to combine the bone formation potential to this 50 % IKVAV hydrogel, a ceramic component such as hydroxyapatite or calcium phosphate can be added to the final formulation. This would form a polymeric-ceramic composite scaffold, where the polymeric phase will be responsible for the induction of angiogenesis and innervation, while the calcium phosphate components will support osteoconduction.

In general, this would dictate a new technological approach for lifting technical barriers in the field of bone tissue engineering and for developing innovative biomaterials providing a microenvironment suitable for bone formation, nerves recruitment and blood vessel invasion.

5. Conclusions

We produced functional hydrogels containing ELP-M(alkene)-40, SH-PEG and a synthetic peptide bearing IKVAV adhesion sequence. These hydrogels had fine-tunable rheological properties, were

degradable *in vitro* and had microporous structure. The biological evaluation showed that these hydrogels could support MSCs, ECs and SNs cultures. The 50 % IKVAV composition induced upregulation of osteogenic markers and genes related to bone repair in MSCs, upregulation of *Tek* in ECs, and a more complex neurite network and longest average neurite length in SNs. *In vivo*, this same composition did not present signals of major inflammation and induced angiogenesis and innervation surrounding the implant.

6. Declaration of Interest

Authors declare no conflict of interest.

7. Acknowledgements

The authors thank Christel Poujol, Sébastien Marais, Fabrice Cordelières and Patrice Mascalchi from the Bordeaux Imaging Center for the support with the histological slides scanning. Philippe Legros from PLACAMAT (Plateforme Aquitaine de caractérisation des matériaux) for the SEM analysis. Sylvie Rey for the histological support. This work was supported by funding from Bordeaux Consortium for Regenerative Medicine (BxCRM), Medical Research Foundation (FRM) dossier FRM SPF20170938783, Aquitaine Region (2016-1R30403), French National Institute of Health and Medical Research (Inserm), University of Bordeaux, National Centre for Scientific Research (CNRS), Polytechnic Institute of Bordeaux (IPB).

8. References

[1] F.M.R. Witjas, B.M. van den Berg, C.W. van den Berg, M.A. Engelse, T.J. Rabelink, Concise Review: The Endothelial Cell Extracellular Matrix Regulates Tissue Homeostasis and Repair, Stem Cells Transl Med (2018).
[2] A. Kumar, J.P. Brockes, Nerve dependence in tissue, organ, and appendage regeneration, Trends Neurosci 35(11) (2012) 691-9.
[3] A.R. Barker, G.D. Rosson, A.L. Dellon, Wound healing in denervated tissue, Ann Plast Surg 57(3) (2006) 339-42.
[4] B. Bakhshandeh, P. Zarrintaj, M.O. Oftadeh, F. Keramati, H. Fouladiha, S. Sohrabi-Jahromi, Z. Ziraksaz, Tissue engineering; strategies, tissues, and biomaterials, Biotechnol Genet Eng Rev 33(2) (2017) 144-172.

[5] L.H. Nguyen, N. Annabi, M. Nikkhah, H. Bae, L. Binan, S. Park, Y. Kang, Y. Yang, A. Khademhosseini, Vascularized bone tissue engineering: approaches for potential improvement, Tissue Eng Part B Rev 18(5) (2012) 363-82.
[6] C. Chenu, Role of innervation in the control of bone remodeling, J Musculoskelet Neuronal Interact 4(2) (2004) 132-4.
[7] S.G. Grassel, The role of peripheral nerve fibers and their neurotransmitters in cartilage and bone physiology and pathophysiology, Arthritis Res Ther 16(6) (2014) 485.
[8] T. Fukuda, S. Takeda, R. Xu, H. Ochi, S. Sunamura, T. Sato, S. Shibata, Y. Yoshida, Z. Gu, A. Kimura, C. Ma, C. Xu, W. Bando, K. Fujita, K. Shinomiya, T. Hirai, Y. Asou, M. Enomoto, H. Okano, A. Okawa, H. Itoh, Sema3A regulates bone-mass accrual through sensory innervations, Nature 497(7450) (2013) 490-3.
[9] D.I. Silva, B.P.D. Santos, J. Leng, H. Oliveira, J. Amedee, Dorsal root ganglion neurons regulate the transcriptional and translational programs of osteoblast differentiation in a microfluidic platform, Cell Death Dis 8(12) (2017) 3209.
[10] R.E. Tomlinson, Z. Li, Q. Zhang, B.C. Goh, Z. Li, D.L.J. Thorek, L. Rajbhandari, T.M. Brushart, L. Minichiello, F. Zhou, A. Venkatesan, T.L. Clemens, NGF-TrkA Signaling by Sensory Nerves Coordinates the Vascularization and Ossification of Developing Endochondral Bone, Cell Rep 16(10) (2016) 2723-2735.
[11] I. Nemec, V. Smrcka, J. Pokorny, The Effect of Sensory Innervation on the Inorganic Component of Bones and Teeth; Experimental Denervation - Review, Prague Med Rep 119(4) (2018) 137-147.
[12] D. Song, X. Jiang, S. Zhu, W. Li, A. Khadka, J. Hu, Denervation impairs bone regeneration during distraction osteogenesis in rabbit tibia lengthening, Acta Orthop 83(4) (2012) 406-10.
[13] K.E. Inostroza-Brito, E.C. Collin, A. Majkowska, S. Elsharkawy, A. Rice, A.E. Del Río Hernández, X. Xiao, J. Rodríguez-Cabello, A. Mata, Cross-linking of a biopolymer-peptide co-assembling system, Acta Biomater 58 (2017) 80-89.
[14] Y.N. Zhang, R.K. Avery, Q. Vallmajo-Martin, A. Assmann, A. Vegh, A. Memic, B.D. Olsen, N. Annabi, A. Khademhosseini, A Highly Elastic and Rapidly Crosslinkable Elastin-Like Polypeptide-Based Hydrogel for Biomedical Applications, Adv Funct Mater 25(30) (2015) 4814-4826.
[15] J.C. Rodríguez-Cabello, L. Martín, M. Alonso, F.J. Arias , A.M. Testera, “Recombinamers” as advanced materials for the post-oil age, Polymer 50(22) (2009) 5159-69.
[16] D.E. Meyer, A. Chilkoti, Purification of recombinant proteins by fusion with thermally-responsive polypeptides, Nat Biotechnol 17(11) (1999) 1112-5.
[17] J.R. McDaniel, D.C. Radford, A. Chilkoti, A unified model for de novo design of elastin-like polypeptides with tunable inverse transition temperatures, Biomacromolecules 14(8) (2013) 2866-72.
[18] W.F. Daamen, J.H. Veerkamp, J.C. van Hest, T.H. van Kuppevelt, Elastin as a biomaterial for tissue engineering, Biomaterials 28(30) (2007) 4378-98.
[19] G.C. Yeo, B. Aghaei-Ghareh-Bolagh, E.P. Brackenreg, M.A. Hiob, P. Lee, A.S. Weiss, Fabricated Elastin, Adv Healthc Mater 4(16) (2015) 2530-2556.
[20] R. Petitdemange, E. Garanger, L. Bataille, W. Dieryck, K. Bathany, B. Garbay, T.J. Deming, S. Lecommandoux, Selective Tuning of Elastin-like Polypeptide Properties via Methionine Oxidation, Biomacromolecules 18(2) (2017) 544-550.
[21] J.R. Kramer, R. Petitdemange, L. Bataille, K. Bathany, A.L. Wirotius, B. Garbay, T.J. Deming, E. Garanger, S. Lecommandoux, Quantitative Side-Chain Modifications of Methionine-Containing Elastin-Like Polypeptides as a Versatile Tool to Tune Their Properties, ACS Macro Lett. 4(11) (2015) 1283–86.
[22] R. Petitdemange, E. Garanger, L. Bataille, K. Bathany, B. Garbay, T.J. Deming, S. Lecommandoux, Tuning Thermoresponsive Properties of Cationic Elastin-like Polypeptides by Varying Counterions and Side-Chains, Bioconjug Chem 28(5) (2017) 1403-1412.
[23] D.L. Gilbert, S.W. Kim, Macromolecular release from collagen monolithic devices, J Biomed Mater Res 24(9) (1990) 1221-39.

[24] C.L. Wang, T. Miyata, B. Weksler, A.L. Rubin, K.H. Stenzel, Collagen-induced platelet aggregation and release. I Effects of side-chain modifications and role of arginyl residues, Biochim Biophys Acta 544(3) (1978) 555-67.
[25] S.A. Malin, B.M. Davis, D.C. Molliver, Production of dissociated sensory neuron cultures and considerations for their use in studying neuronal function and plasticity, Nat Protoc 2(1) (2007) 152-60.
[26] J. O'Brien, I. Wilson, T. Orton, F. Pognan, Investigation of the Alamar Blue (resazurin) fluorescent dye for the assessment of mammalian cell cytotoxicity, Eur J Biochem 267(17) (2000) 5421-6.
[27] D. Koch, W.J. Rosoff, J. Jiang, H.M. Geller, J.S. Urbach, Strength in the periphery: growth cone biomechanics and substrate rigidity response in peripheral and central nervous system neurons, Biophys J 102(3) (2012) 452-60.
[28] X. Ren, Y. Feng, J. Guo, H. Wang, Q. Li, J. Yang, X. Hao, J. Lv, N. Ma, W. Li, Surface modification and endothelialization of biomaterials as potential scaffolds for vascular tissue engineering applications, Chem Soc Rev 44(15) (2015) 5680-742.
[29] P. Liesi, A. Närvänen, J. Soos, H. Sariola, G. Snounou, Identification of a neurite outgrowth-promoting domain of laminin using synthetic peptides, FEBS Lett 244(1) (1989) 141-8.
[30] K. Tashiro, G.C. Sephel, B. Weeks, M. Sasaki, G.R. Martin, H.K. Kleinman, Y. Yamada, A synthetic peptide containing the IKVAV sequence from the A chain of laminin mediates cell attachment, migration, and neurite outgrowth, J Biol Chem 264(27) (1989) 16174-82.
[31] R. Patel, M. Santhosh, J.K. Dash, R. Karpoormath, A. Jha, J. Kwak, M. Patel, J.H. Kim, Ile-Lys-Val-ala-Val (IKVAV) peptide for neuronal tissue engineering, Polym Adv Technol 30(1) (2019) 4-12.
[32] X. Lin, K. Takahashi, Y. Liu, P.O. Zamora, Enhancement of cell attachment and tissue integration by a IKVAV containing multi-domain peptide, Biochim Biophys Acta 1760(9) (2006) 1403-10.
[33] M.C. Kibbey, M.L. Corcoran, L.M. Wahl, H.K. Kleinman, Laminin SIKVAV peptide-induced angiogenesis in vivo is potentiated by neutrophils, J Cell Physiol 160(1) (1994) 185-93.
[34] M.C. Kibbey, D.S. Grant, H.K. Kleinman, Role of the SIKVAV site of laminin in promotion of angiogenesis and tumor growth: an in vivo Matrigel model, J Natl Cancer Inst 84(21) (1992) 1633-8.
[35] J.E. Frith, R.J. Mills, J.E. Hudson, J.J. Cooper-White, Tailored integrin-extracellular matrix interactions to direct human mesenchymal stem cell differentiation, Stem Cells Dev 21(13) (2012) 2442-56.
[36] Pate R, Santhosh M, Dash JK, Karpoormath R, Jha A, Kwak J, Patel M, H.K. JH., Ile-Lys-Val-ala-Val (IKVAV) peptide for neuronal tissue engineering, Polym Adv Technol 30(1) (2019) 4-12.
[37] X. Guan, M. Avci-Adali, E. Alarçin, H. Cheng, S.S. Kashaf, Y. Li, A. Chawla, H.L. Jang, A. Khademhosseini, Development of hydrogels for regenerative engineering, Biotechnol J 12(5) (2017).
[38] K. Whang, K.E. Healy, D.R. Elenz, E.K. Nam, D.C. Tsai, C.H. Thomas, G.W. Nuber, F.H. Glorieux, R. Travers, S.M. Sprague, Engineering bone regeneration with bioabsorbable scaffolds with novel microarchitecture, Tissue Eng 5(1) (1999) 35-51.
[39] C.G. Williams, A.N. Malik, T.K. Kim, P.N. Manson, J.H. Elisseeff, Variable cytocompatibility of six cell lines with photoinitiators used for polymerizing hydrogels and cell encapsulation, Biomaterials 26(11) (2005) 1211-8.
[40] Y. Yamaguchi, J. Ohno, A. Sato, H. Kido, T. Fukushima, Mesenchymal stem cell spheroids exhibit enhanced in-vitro and in-vivo osteoregenerative potential, BMC Biotechnol 14 (2014) 105.
[41] B. Gurumurthy, P.C. Bierdeman, A.V. Janorkar, Spheroid model for functional osteogenic evaluation of human adipose derived stem cells, J Biomed Mater Res A 105(4) (2017) 1230-1236.
[42] J. Raphel, J. Karlsson, S. Galli, A. Wennerberg, C. Lindsay, M.G. Haugh, J. Pajarinen, S.B. Goodman, R. Jimbo, M. Andersson, S.C. Heilshorn, Engineered protein coatings to improve the osseointegration of dental and orthopaedic implants, Biomaterials 83 (2016) 269-82.
[43] M.T. Valenti, L. Dalle Carbonare, M. Mottes, Osteogenic Differentiation in Healthy and Pathological Conditions, Int J Mol Sci 18(1) (2016).
[44] Q. Chen, P. Shou, C. Zheng, M. Jiang, G. Cao, Q. Yang, J. Cao, N. Xie, T. Velletri, X. Zhang, C. Xu, L. Zhang, H. Yang, J. Hou, Y. Wang, Y. Shi, Fate decision of mesenchymal stem cells: adipocytes or osteoblasts?, Cell Death Differ 23(7) (2016) 1128-39.

[45] S. Patel-Hett, P.A. D'Amore, Signal transduction in vasculogenesis and developmental angiogenesis, Int J Dev Biol 55(4-5) (2011) 353-63.
[46] F. Mackenzie, C. Ruhrberg, Diverse roles for VEGF-A in the nervous system, Development 139(8) (2012) 1371-80.
[47] Z. Zhong, H. Gu, J. Peng, W. Wang, B.H. Johnstone, K.L. March, M.R. Farlow, Y. Du, GDNF secreted from adipose-derived stem cells stimulates VEGF-independent angiogenesis, Oncotarget 7(24) (2016) 36829-36841.
[48] M.S. Airaksinen, M. Saarma, The GDNF family: signalling, biological functions and therapeutic value, Nat Rev Neurosci 3(5) (2002) 383-94.
[49] A. Hattori, M. Katayama, S. Iwasaki, K. Ishii, M. Tsujimoto, M. Kohno, Bone morphogenetic protein-2 promotes survival and differentiation of striatal GABAergic neurons in the absence of glial cell proliferation, J Neurochem 72(6) (1999) 2264-71.
[50] C. Zhang, C. Meng, D. Guan, F. Ma, BMP2 and VEGF165 transfection to bone marrow stromal stem cells regulate osteogenic potential in vitro, Medicine (Baltimore) 97(5) (2018) e9787.
[51] M. Bosetti, L. Fusaro, E. Nicolì, A. Borrone, S. Aprile, M. Cannas, Poly-L-lactide acid-modified scaffolds for osteoinduction and osteoconduction, J Biomed Mater Res A 102(10) (2014) 3531-9.
[52] B. Li, T. Qiu, P. Zhang, X. Wang, Y. Yin, S. Li, IKVAV regulates ERK1/2 and Akt signalling pathways in BMMSC population growth and proliferation, Cell Prolif 47(2) (2014) 133-45.
[53] M. Bruderer, R.G. Richards, M. Alini, M.J. Stoddart, Role and regulation of RUNX2 in osteogenesis, Eur Cell Mater 28 (2014) 269-86.
[54] Y.H. Choi, Y.M. Gu, J.W. Oh, K.Y. Lee, Osterix is regulated by Erk1/2 during osteoblast differentiation, Biochem Biophys Res Commun 415(3) (2011) 472-8.
[55] C.C. Mandal, H. Drissi, G.G. Choudhury, N. Ghosh-Choudhury, Integration of phosphatidylinositol 3-kinase, Akt kinase, and Smad signaling pathway in BMP-2-induced osterix expression, Calcif Tissue Int 87(6) (2010) 533-40.
[56] C. Ge, G. Xiao, D. Jiang, Q. Yang, N.E. Hatch, H. Roca, R.T. Franceschi, Identification and functional characterization of ERK/MAPK phosphorylation sites in the Runx2 transcription factor, J Biol Chem 284(47) (2009) 32533-43.
[57] J. Guerrero, S. Catros, S.M. Derkaoui, C. Lalande, R. Siadous, R. Bareille, N. Thebaud, L. Bordenave, O. Chassande, C. Le Visage, D. Letourneur, J. Amedee, Cell interactions between human progenitor-derived endothelial cells and human mesenchymal stem cells in a three-dimensional macroporous polysaccharide-based scaffold promote osteogenesis, Acta Biomater 9(9) (2013) 8200-13.
[58] J. Guerrero, H. Oliveira, R. Aid, R. Bareille, R. Siadous, D. Letourneur, Y. Mao, J. Kohn, J. Amedee, Influence of the three-dimensional culture of human bone marrow mesenchymal stromal cells within a macroporous polysaccharides scaffold on Pannexin 1 and Pannexin 3, J Tissue Eng Regen Med 12(4) (2018) e1936-e1949.
[59] J. van Weerd, M. Karperien, P. Jonkheijm, Supported Lipid Bilayers for the Generation of Dynamic Cell-Material Interfaces, Adv Healthc Mater 4(18) (2015) 2743-79.
[60] Y. Chen , J. Yang, J. Gong, Adhesion, Spreading, and Proliferation of Endothelial Cells on Charged Hydrogels, The Journal of Adhesion 85(11) (2009) 839-868.
[61] D.S. Grant, J.L. Kinsella, R. Fridman, R. Auerbach, B.A. Piasecki, Y. Yamada, M. Zain, H.K. Kleinman, Interaction of endothelial cells with a laminin A chain peptide (SIKVAV) in vitro and induction of angiogenic behavior in vivo, J Cell Physiol 153(3) (1992) 614-25.
[62] R. Liu, G. Lin, H. Xu, An efficient method for dorsal root ganglia neurons purification with a one-time anti-mitotic reagent treatment, PLoS One 8(4) (2013) e60558.
[63] A. Sepehr, J. Ruud, S. Mohseni, Neuron survival in vitro is more influenced by the developmental age of the cells than by glucose condition, Cytotechnology 61(1-2) (2009) 73-9.
[64] T. Repić, K. Madirazza, E. Bektur, D. Sapunar, Characterization of dorsal root ganglion neurons cultured on silicon micro-pillar substrates, Sci Rep 6 (2016) 39560.
[65] A. Ladak, J. Olson, E.E. Tredget, T. Gordon, Differentiation of mesenchymal stem cells to support peripheral nerve regeneration in a rat model, Exp Neurol 228(2) (2011) 242-52.

[66] H. Kim, T. W Caspar, S.B. Shah, A.H. Hsieh, Effects of proinflammatory cytokines on axonal outgrowth from adult rat lumbar dorsal root ganglia using a novel three-dimensional culture system, Spine J 15(8) (2015) 1823-31.
[67] A.W. Harrington, D.D. Ginty, Long-distance retrograde neurotrophic factor signalling in neurons, Nat Rev Neurosci 14(3) (2013) 177-87.
[68] A. Ibáñez-Fonseca, T.L. Ramos, I. González de Torre, L.I. Sánchez-Abarca, S. Muntión, F.J. Arias, M.C. Del Cañizo, M. Alonso, F. Sánchez-Guijo, J.C. Rodríguez-Cabello, Biocompatibility of two model elastin-like recombinamer-based hydrogels formed through physical or chemical cross-linking for various applications in tissue engineering and regenerative medicine, J Tissue Eng Regen Med 12(3) (2018) e1450-e1460.

Figure legends

Figure 1. Description of hydrogels' formation and rheological properties **(A)** Chemical structure of the ELP used in this study. **(B)** Schematic representation of the hydrogel components, photo-irradiation conditions, and a photography of the ELP + PEG hydrogel (scale bar = 1 mm). In brief, hydrogels were produced from the alkene-bearing ELP, 4 arm-thiolayted Poly(ethylene glycol) (4 arm HS-PEG) and adhesion peptides (IKVAV or VKAIV) using equimolar proportion of functional groups (*i.e.*, total thiol to alkene), under photoactivation of Irgacure ® at 0.5 % (w/v) for 8 minutes. **(C)** Hydrogels compositions with the concentration of all components. **(D)** Rheological characterization at 37 °C of the ELP + PEG hydrogel at different final mass concentrations and ELP + 50 % IKVAV and ELP + 50 % VKAIV. Storage modulus (G') of each concentration is indicated.

Figure 2. Hydrogel characterization for all tested compositions. **(A)** Scanning electronic microscopy of ELPM40 + PEG, ELPM40 + 25 % IKVAV, ELPM40 + 25 % VKAIV, ELPM40 + 50 % IKVAV, ELPM40 + 50 % VKAIV showing the microporous structure (scale=10 μm). **(B)** Pore size quantification shows that compositions containing 25 % adhesion peptides are smaller

than the other compositions (Average ± SD, 63<n<85, ***p<0.001). **(C)** Free primary amines in solution were detected for all compositions indicating that photoreticulation process did not interfere in the *in vitro* degradation property. Data are represented as average ± SD, n=6, with statistical differences indicated as *p<0.05, ***p<0.001 (ANOVA with Bonferroni test as post-hoc).

Figure 3. Metabolic activity of bone marrow mesenchymal stromal cells (MSCs), endothelial cells (ECs), and sensory neurons (SNs). Data are represented as average ± SD, n=5, with statistical differences indicated as *p<0.05, **p<0.01 and ***p<0.001 (ANOVA with Bonferroni test as post-hoc).

Figure 4. **(A)** Representative images of rat bone marrow mesenchymal stem cells (MSCs) morphology within the hydrogel compositions. MSCs were labeled with phalloidin (red) and nuclei with DAPI (blue). Further methodological details are described in section 2.7. **(B)** Gene expression after 7 days of culture of MSCs in ELPM40 + PEG, ELPM40 + 25 % IKVAV, ELPM40 + 25 % VKAIV, ELPM40 + 50 % IKVAV and ELPM40 + 50 % VKAIV compositions. Data are represented as average ± SD, n=4, with statistical differences indicated as *p<0.05, **p<0.01 and ***p<0.001 (ANOVA with Bonferroni test as post-hoc). Bars: 100 μm.

Figure 5. **(A)** Representative images of rat bone marrow endothelial cells (ECs) morphology within the hydrogel compositions. ECs were labeled with phalloidin (red) and nuclei with DAPI (blue). Further methodological details are described in section 2.7. **(B)** Gene expression after 7 days of culture of ECs in ELPM40 + PEG, ELPM40 + 25 % IKVAV, ELPM40 + 25 % VKAIV,

ELPM40 + 50 % IKVAV and ELPM40 + 50 % VKAIV compositions. Data are represented as average ± SD, n=5, with statistical differences indicated as *p<0.05 and **p<0.01 (ANOVA with Bonferroni test as post-hoc). Bars=100 µm.

Figure 6. Representative images of sensory neurons morphology within the hydrogel compositions and average neurite length after cultured in ELPM40 + PEG, ELPM40 + 25 % IKVAV, ELPM40 + 50 % IKVAV, ELPM40 + 25 % VKAIV, and ELPM40 + 50 % VKAIV. Neurons were labeled against βIII tubulin (shown in green) and nuclei with DAPI (blue). Further methodological details are described in section 2.7. Data are represented as average ± SD, 5<n<30, with statistical differences indicated as *p<0.05, **p<0.01 and ***p<0.001 (ANOVA with Bonferroni test as post-hoc). Bars=100 µm.

Figure 7. Subcutaneous evaluation of 50 % IKVAV composition and its scrambled after 11 and 26 days. Histological slides were analyzed for i) inflammation potential (HE), ii) ability to induce angiogenesis (immunohistochemistry of CD31) and iii) innervation (immunohistochemistry of βIII tubulin (β3T)). Hydrogel structure is indicated by white asterisks, vessels are indicated by white arrowheads, and hydrogel boundary is indicated by red dashed line. Bars=50 µm for HE and CD31. High magnifications of of CD31 and β3T staining are showed, bars=20 µm.

Figure 8. Quantification of vessels formed in the surrounding area of implantation of 50 % IKVAV composition and its scrambled VKAIV. Data are represented as average ± SD, 3<n<6, with statistical differences indicated as *p<0.05 (ANOVA with Bonferroni test as post-hoc).

Table 1. Genes analyzed and primer sequences used.

Gene	Gene ID	Sequence	Fragment length (bp)
Runx2	367218	F: 5' CCTTCCCTCCGAGACCCTAA 3' R: 5' ATGGCTGCTCCCTTCTGAAC 3'	90
Sp7 (Osx)	300260	F: 5' TGCTTGAGGAAGAAGCTCACTA 3' R: 5' GGGGCTGAAAGGTCAGTGTA 3'	148
Spp1 (Opn)	25353	F: 5' GAGTTTGGCAGCTCAGAGGA 3' R: 5’ TCTGCTTCTGAGATGGGTCA 3'	91
Bmp2	29373	F: 5’ CGGACTGCGGTCTCCTAA 3’ R: 5’ GGGGAAGCAGCAACACTAGA 3’	68
Vegfa	83785	F: 5’ CTTCTTCCACCACTGTGTCT 3’ R: 5’ GCCTCAGGACATGGCACTAT 3’	200
Angpt1	89807	F: 5’ GCTAACAGGAGGTTGGTGGT 3’ R: 5’ CACTTTATCCCATTCAGTTTTCCA 3’	102
Mmp2	81686	F: 5’ CCCTCCCCTGATGCTGATAC 3’ R: 5’ CTGTCCGCCAAATAAACCGAT 3’	157
Tek (Tie-2)	89804	F: 5’ CCACAGATAGAGGATTTGCCAG 3’ R: 5’ AAGTCATTTGGTTGGAGCACTG 3’	146
Rplp0	64205	F: 5' CACTGGCTGAAAAGGTCAAGG 3' R: 5' GTGTGAGGGGCTTAGTCGAA 3'	187

Figure 1

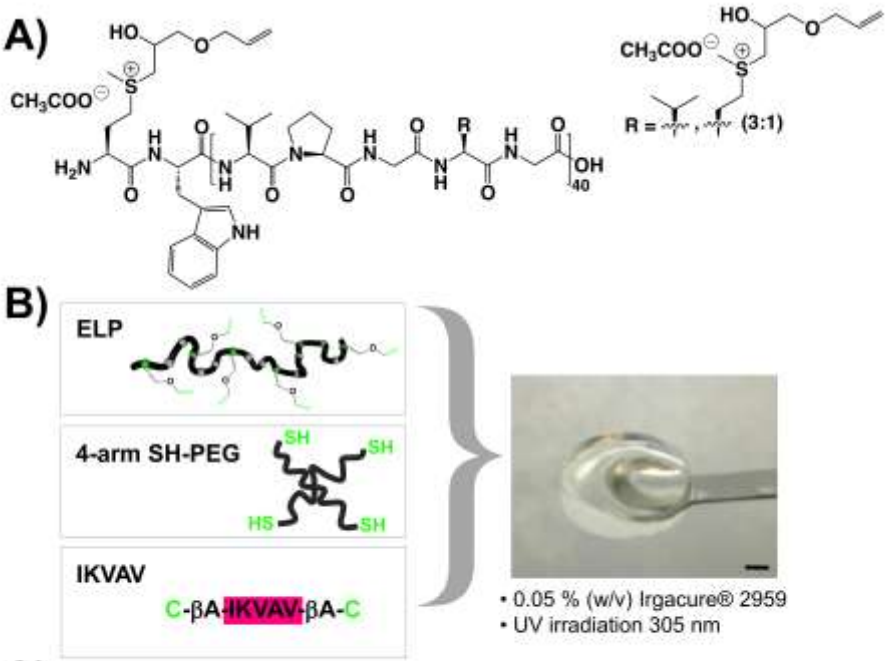

C)

Hydrogel composition	Components	% (w/total w)	Concentration (mM)
ELPM40 + PEGSH	ELPM40	26.3	1 .1
	PEGSH	73.7	2.8
ELPM40 + (**adhesion peptide 25 %** + PEGSH 75 %)	ELPM40	32.1	1.3
	Adh peptide	1.9	1.7
	PEGSH	66	2.5
ELPM40 + (**adhesion peptide 50 %** + PEGSH 50 %)	ELPM40	40.1	1.7
	Adh peptide	4.9	4.1
	PEGSH	55.1	2.1

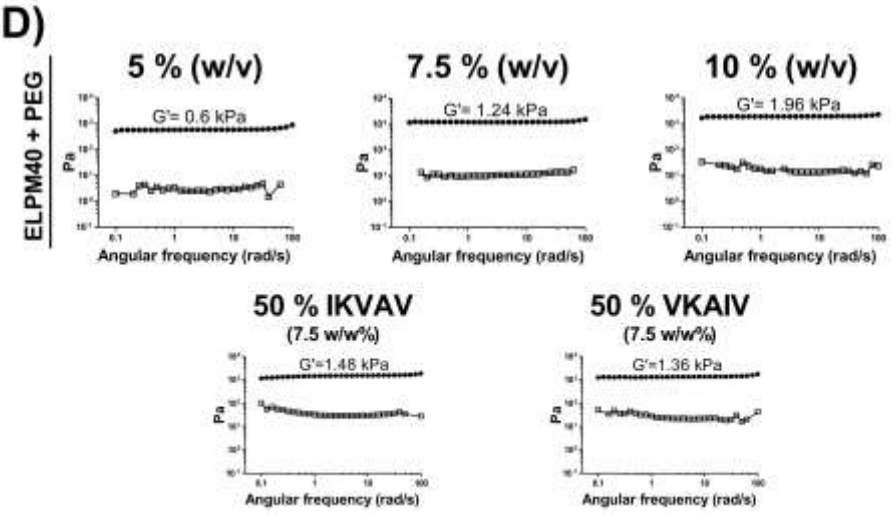

Figure 2

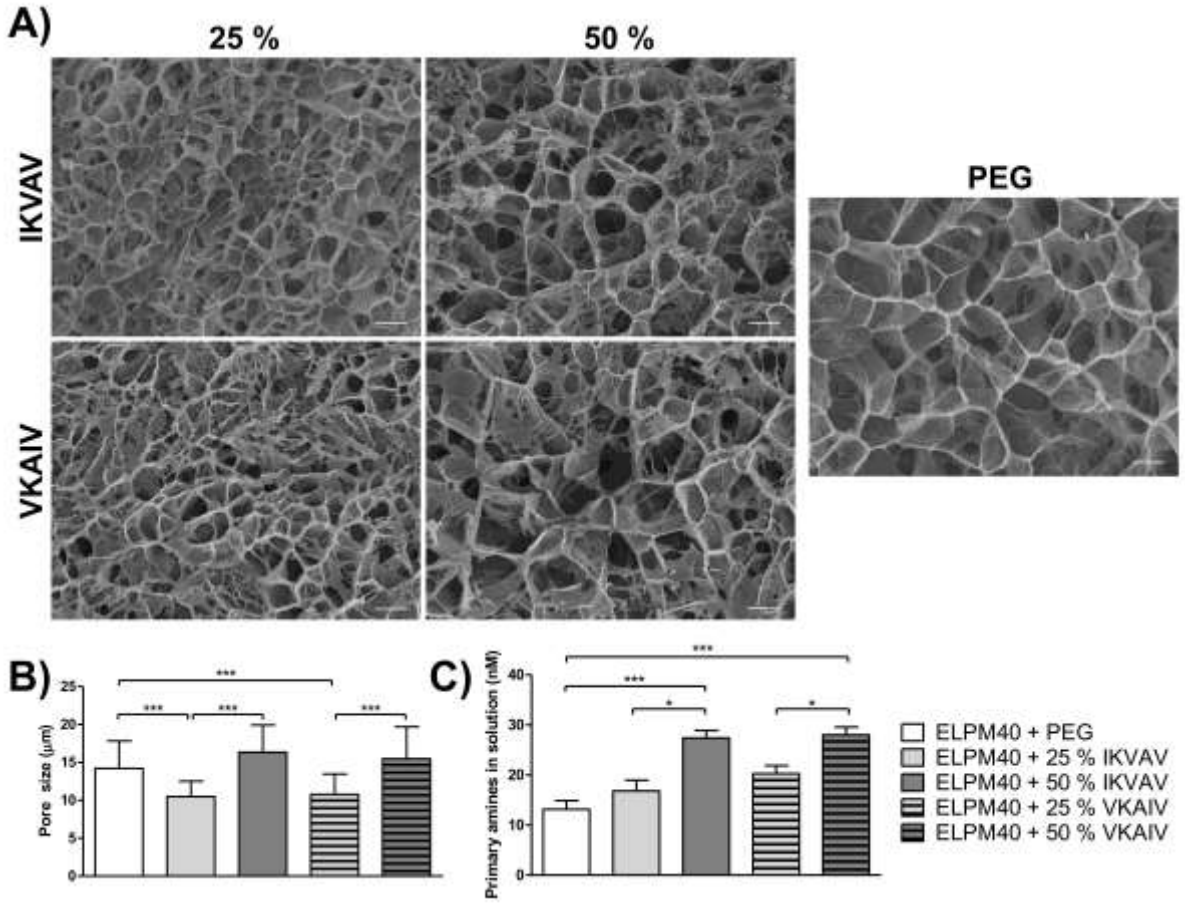

Figure 3

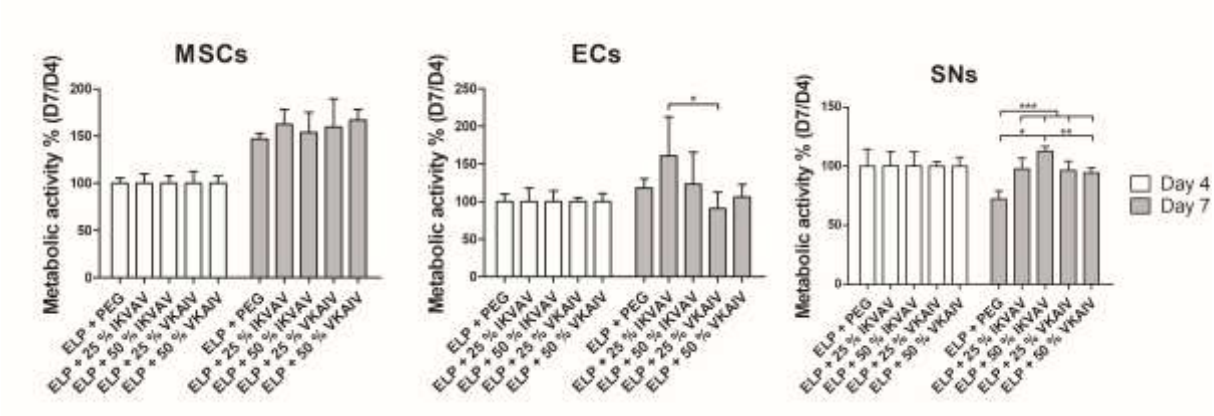

Figure 4

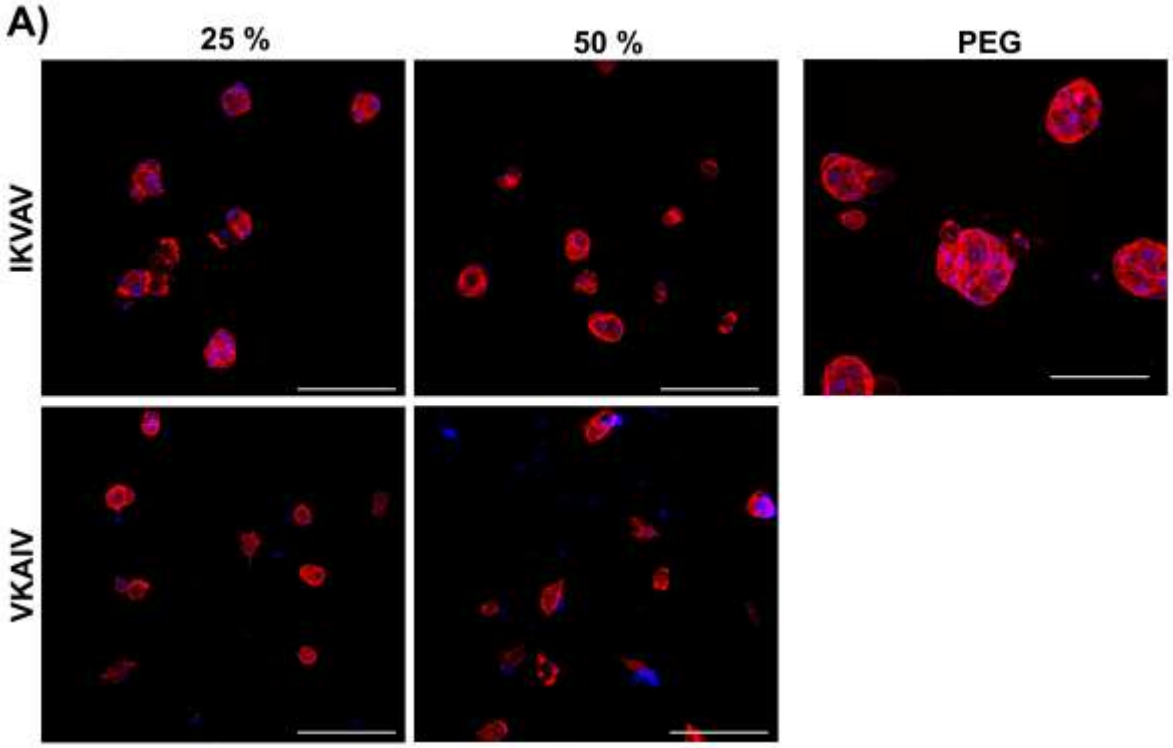
A)
25 %
50 %
PEG
IKVAV
VKAIV

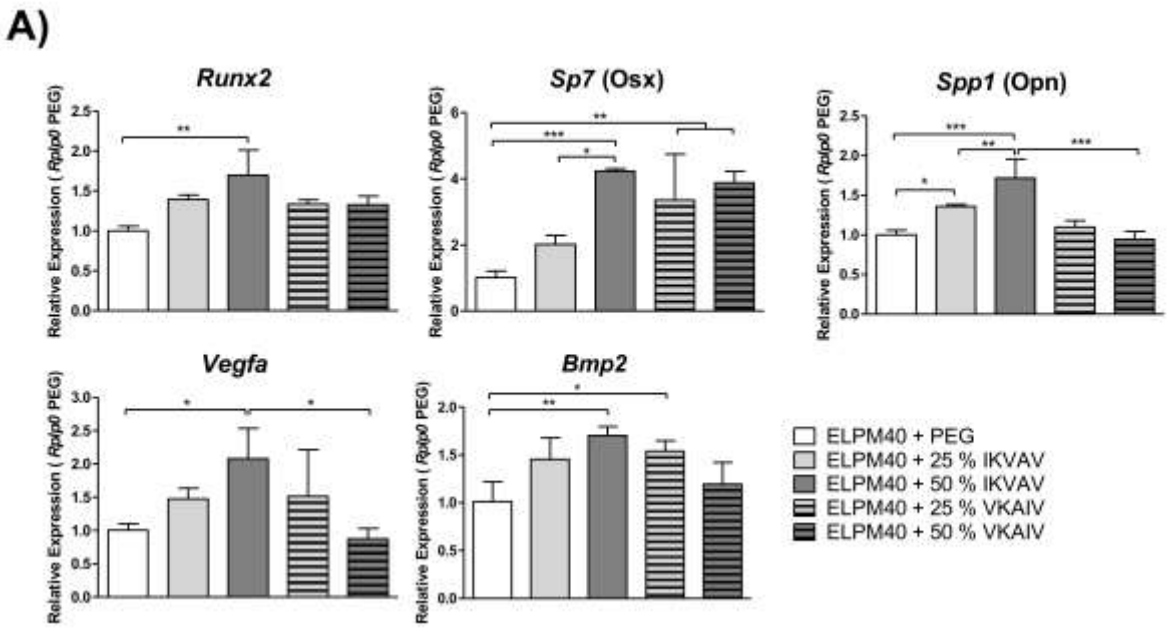
A)
Runx2
Sp7 (Osx)
Spp1 (Opn)
Vegfa
Bmp2
Relative Expression (Rplp0 PEG)
ELPM40 + PEG
ELPM40 + 25 % IKVAV
ELPM40 + 50 % IKVAV
ELPM40 + 25 % VKAIV
ELPM40 + 50 % VKAIV

Figure 5

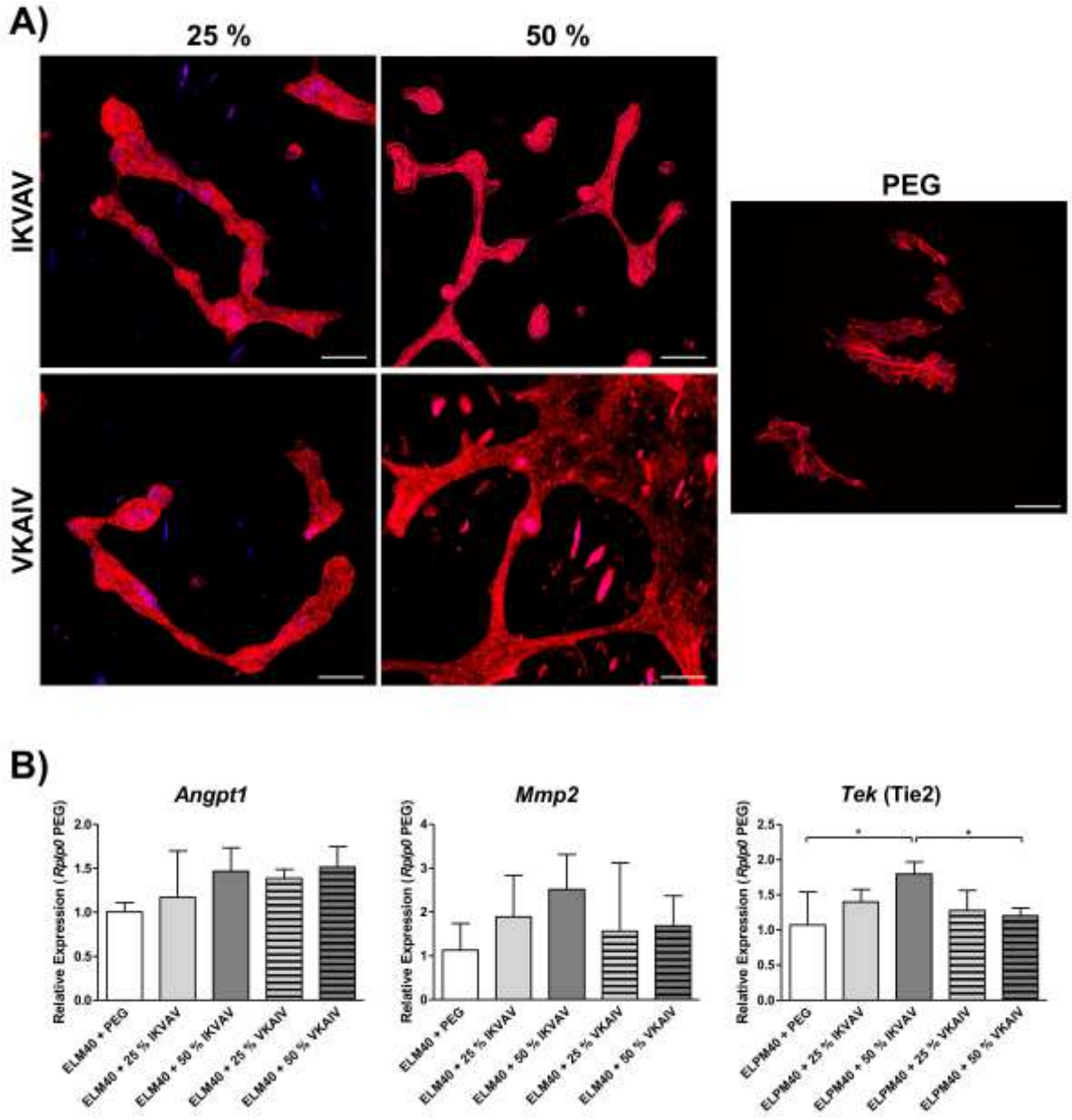
A)
25 %
50 %
IKVAV
VKAIV
PEG
B)
Angpt1
Mmp2
Tek (Tie2)
Relative Expression (Rplp0 PEG)
ELM40 + PEG
ELM40 + 25 % IKVAV
ELM40 + 50 % IKVAV
ELM40 + 25 % VKAIV
ELM40 + 50 % VKAIV
ELPM40 + PEG
ELPM40 + 25 % IKVAV
ELPM40 + 50 % IKVAV
ELPM40 + 25 % VKAIV
ELPM40 + 50 % VKAIV

Figure 6

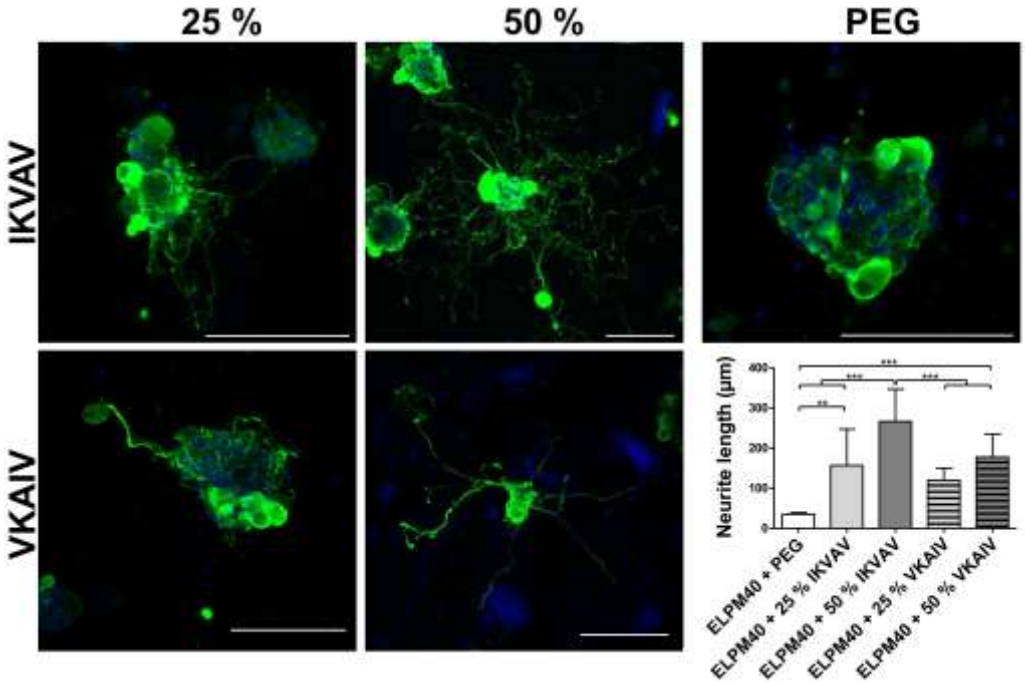

Figure 7

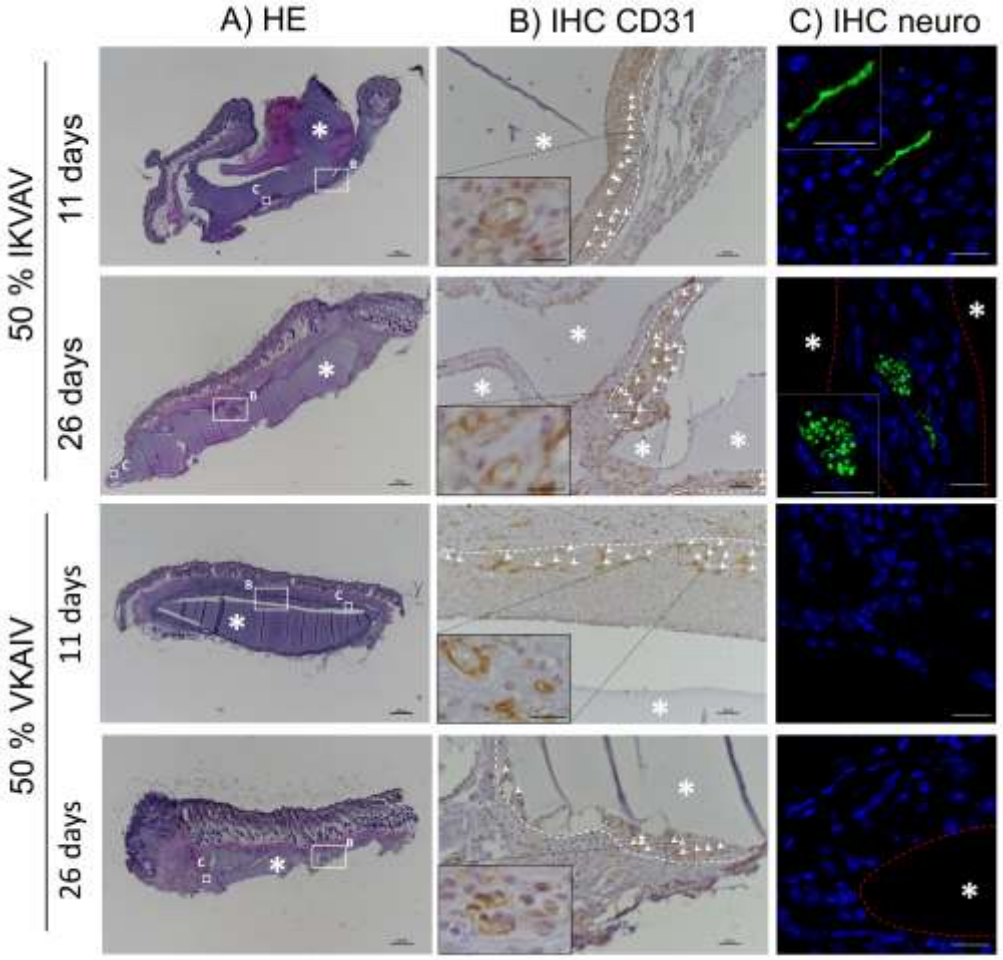

Figure 8

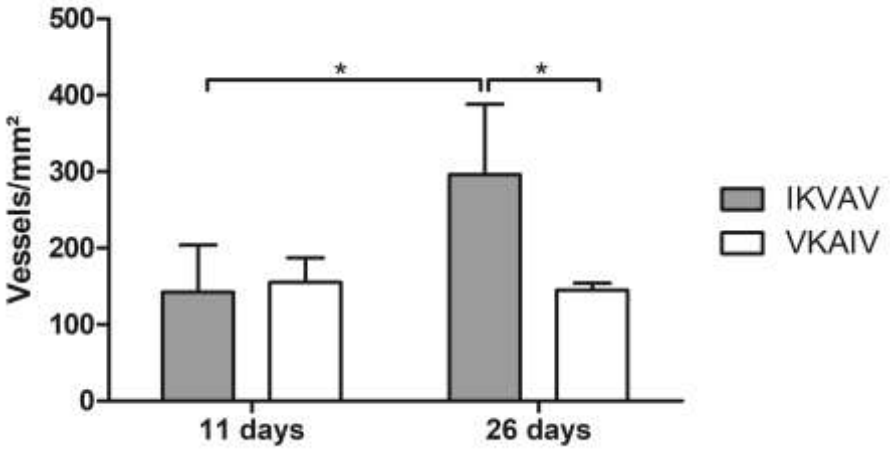

Author manuscript of article published in Acta Biomateriala 99, 154-167 (2019) DOI: 10.1016/j.actbio.2019.08.028

SUPPLEMENTARY DATA

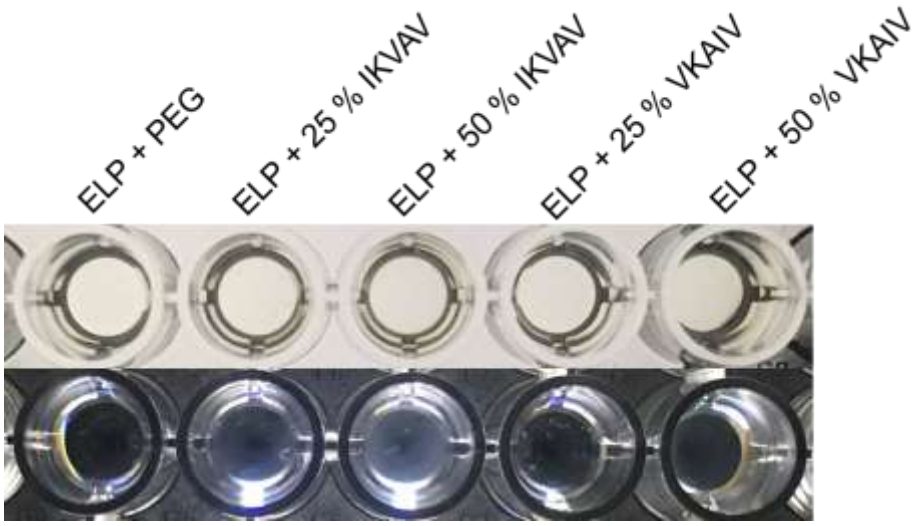

Supplementary Figure 1. Photomicrography of all hydrogel compositions tested. Hydrogels were produced in 96 well plate and photos were taken in bright field with a white (on the top) and with a black background (on the bottom). Note that all compositions provided transparent hydrogels.

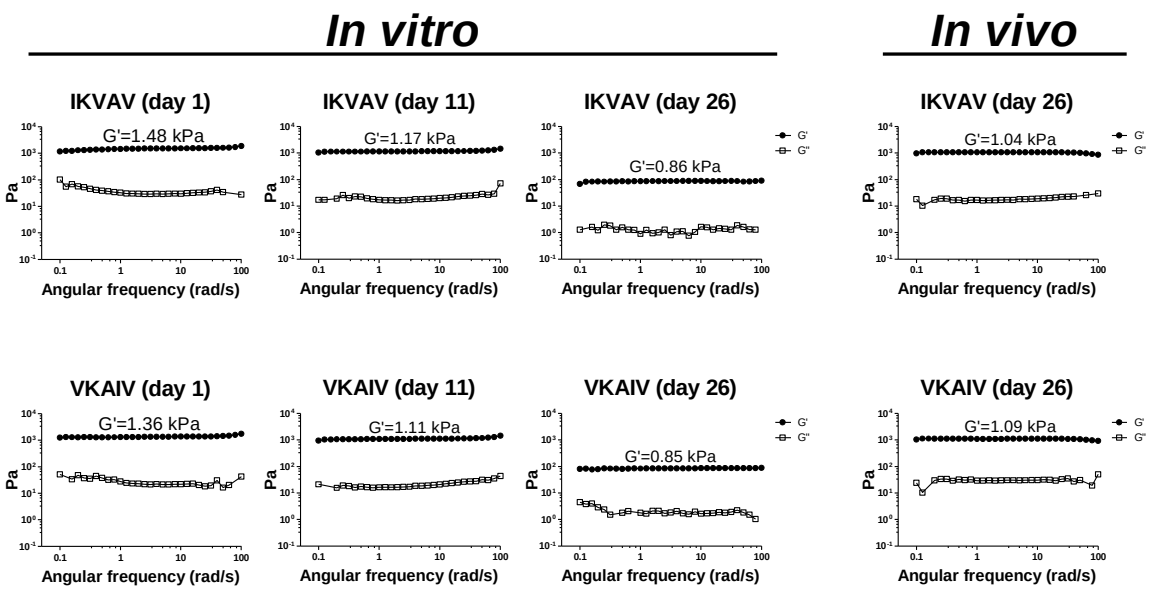

Supplementary Figure 2. Rheological analysis of 50 % IKVAV and 50 % VKAIV compositions after 1, 11 and 26 days of incubation at 37 °C in PBS 0.01 M and after 26 days of subcutaneously implantation in 9 weeks old female Balb/c mice (n=2 for each group). Note that there is a decrease in storage modulus over time but they remain similar in IKVAV and VKAIV compositions at the same time point.